JOURNAL OF SOLID STATE CHEMISTRY **129,** 346–359 (1997)
ARTICLE NO. SC967263

Analysis and Structural Determination of Nd-Substituted Zirconolite-4M

A. A. Coelho, R. W. Cheary, and K. L. Smith*

Faculty of Science, University of Technology, Sydney, Broadway, Sydney, New South Wales, Australia 2007; and
**Advanced Materials Program, ANSTO, Lucas Heights, PMB1, NSW 2234, Australia*

Received August 19, 1996; accepted December 10, 1996

The structure of a new polytype of zirconolite, zirconolite-4M, has been determined using X-ray and neutron powder diffraction, high resolution transmission electron microscopy, and selected area electron diffraction. Zirconolite-4M occurs when zirconolite is doped with 0.5–0.8 Nd per formula unit. Its structure consists of four hexagonal tungsten bronze (HTB) type layers interleaved alternately with layers of Ca, Zr polyhedra (as in zirconolite-2M) and Ca, Ti polyhedra (as in pyrochlore). Nd substitutes on the Ca and Zr sites. The compositions of the zirconolites were determined using an extrapolation technique based on an analysis of the impurity lines in the diffraction pattern. Cation site occupancies were determined with composition constraints applied and these were consistent with the expected zirconolite-4M cation site occupancies. Observed zirconolite-4M lattice parameters correlated with expected values for a zirconolite and pyrochlore type stacking sequence. © 1997 Academic Press

INTRODUCTION

A key aspect of the development of a ceramic host material for high level nuclear waste is the effectiveness of the immobilization of radioactive lanthanide elements in the wasteform. These elements have long half-lives and constitute a significant proportion of the waste. In the multiphase titanate wasteform known as Synroc (1), the lanthanides are immobilized in solid solution within the zirconolite phase $CaZr_xTi_{3-x}O_7$ and in the perovskite phase $CaTiO_3$ (2). The principal reasons for including zirconolite in Synroc is that it occurs naturally with significant proportions of crystallochemically bound uranium and thorium (3) and is known to have withstood the long term effects of high level doses of alpha radiation without significant degradation (4). In the present paper we have investigated how zirconolite accommodates neodymium Nd^{3+}, one of the largest of the trivalent elements in the lanthanide group, at concentrations between 0.5 and 0.8 Nd per formula unit. Within this range we have identified a new polytype of zirconolite, described as zirconolite-4M. This polytype has only been identified previously on a small scale either as an intergrowth phase (2) or as a minor phase in a multiphase specimen (6).

When the Ca in zirconolite $CaZr_xTi_{3-x}O_7$ is replaced by one of the trivalent rare earth elements (REEs) from Nd to Yb, various polytypes of zirconolite form depending on the level of substitution and the temperature of preparation (7, 8). Within all zirconolites there are two basic layer units which pack next to each other parallel to the (001). One of these layers consists of Ti–O polyhedra which approximate an hexagonal tungsten bronze (HTB) motif. In between the HTB layers are layers of Ca and Zr polyhedra (9–11). The different polytypes are characterized by the way in which the layers of the zirconolite are stacked together and by the number of HTB layers in a repeat sequence. In its unsubstituted state or at low levels of substituted REE (i.e., $< \sim 0.2$ per formula unit), zirconolite consists of two HTB layers and two layers of Ca and Zr polyhedra. In these circumstances the lattice is monoclinic, the space group $C2/c$ (9, 11, 12), and the structure is referred to as zirconolite-2M (using the nomenclature of the International Mineralogical Association Commission on New Minerals and Mineral Names Pyrochlore Subcommittee (13)). Another of the polytypes associated with Nd substitution is zirconolite-3T which is trigonal and consists of three HTB layers separated by layers of Ca and Zr polyhedra (7, 14). This phase tends to form at slightly higher levels of Nd substitution than the zirconolite-2M polytype. At high levels of REE substitution, zirconolite converts into cubic pyrochlore (e.g., $Nd_2(Ti/Zr)_2O_7$). Both the zirconolite-2M and pyrochlore structures are fluorite (CaF_2) derivatives with the cations at approximately the same positions as in the parent fluorite structure. The major difference between the two structures is the ordering of the cations, and the displacement of the oxygen anions from their ideal fluorite positions.

Under certain conditions we have observed that zirconolites can form with REE concentrations greater than that for zirconolite-3T and less than that for pyrochlore. In this work, we have been able to prepare enough single-phase

0022-4596/97 $25.00

polycrystalline specimens of this new phase and carry out a structural analysis using simultaneous Rietveld refinement on high resolution neutron powder diffraction data and X-ray powder diffraction data. The structure determined is made up of four HTB-type layers interlaced alternately with layers of Ca, Zr polyhedra (like those found in zirconolite-2M) and layers of Ca, Ti polyhedra (like those found in pyrochlore). Nd substitutes on the Ca and Zr sites. We call this new phase zirconolite-4M.

Preliminary fits to X-ray diffraction data using a 2M structural model were good which implies that the 4M cation positions are very similar to the 2M positions. However, 2M "forbidden" reflections were observed, indicating either lower symmetry or an enlarged unit cell. Neutron diffraction fits using the 2M model were very poor which implies that the 4M anion positions are clearly different from the 2M model. High resolution TEM images and SAD patterns of 4M specimens showed a four-layer repeat unit of $\sim$22 Å (6). These observations indicate that the 2M model is clearly inadequate for describing the 4M phase. A 4M model based on the 2M cation positions was developed using X-ray and neutron diffraction data which is consistent with the HRTEM images.

THE CRYSTAL STRUCTURE AND HTB STACKING IN ZIRCONOLITES AND PYROCHLORE

The crystal structures of zirconolite-2M and pyrochlore are shown in Fig. 1. They are similar in that they are both layer structures and that alternate layers are primarily composed of octahedrally coordinated cations.

Zirconolite-2M. In the idealized description of zirconolite, adjacent HTB layers at $z = 0.25$ and 0.75 are related by a 180° rotation around the **c*** axis and an offset of 2.1 Å in the [130] direction. The relationship between layers at $z = 0.75$ and 1.25 is similar except that the offset is in the $[1\bar{3}0]$ direction. In this structure the CaO_8 polyhedra form as distorted cubes with an average Ca–O bond length of approximately 2.45 Å. The Zr sites within the ZrO_7 polyhedra are occupied mainly by Zr and Ti ions with the Zr–O bond length averaging out at 2.17 Å. Of the Ti sites, both the Ti(1) and Ti(3) sites are octahedrally coordinated and occupied predominantly by Ti ions, whereas the Ti(2) site is split into two off-center sites of fivefold coordination about 0.6 Å apart, each with a statistical occupancy level of 50%.

Zirconolite-3T. The data presented by Mazzi and Munno (14) describe cation polyhedra that are virtually identical to those of the 2M structure, including the statistically distributed split Ti(2) site. In contrast to the one Ca site occurring in the 2M structure, the 3T structure has two Ca sites originating from symmetry considerations. The Ca and Zr atoms, as in 2M, are arranged in rows parallel to [110] at $z = 0$, [100] at $z = \frac{1}{3}$, and [010] at $z = \frac{2}{3}$ with the offset between adjacent layers similar to the 2M case. Adjacent HTB layers are related by a 120° rotation with the **a** and **b** lattice parameters exhibiting perfect hexagonal symmetry.

Pyrochlore. The oxide pyrochlore $[Ca, Zr, REE]_2^{VIII} Ti_2^{VI} O_7$ or $A_2^{VIII} B_2^{VI} X_6 Y$, like zirconolite, is an anion-deficient structure derived from the cubic fluorite structure. The eightfold coordinated A cations are bonded to six X anions at $\sim$2.69 Å and two Y anions at $\sim$2.26 Å. The B cations bond with six X anions and form a three-dimensional octahedral framework. The structure can be described as two interpenetrating three-dimensional networks of A_2Y and B_2X_6 nets (15). The description given here will concentrate on the similarities between pyrochlore and zirconolite. Parallel to (111), pyrochlore is composed of two types of layers stacked one on top of the other (see Fig. 1e–f). One of the layers is a HTB-type layer predominantly composed of octahedrally coordinated ions. The other layer is predominantly composed of ions in eight-fold coordination. Individual pyrochlore HTB layers are very similar to those of zirconolite. The main difference is the replacement of the split Ti sites with A cations.

Two quantities can be used to describe the stacking sequences of successive HTB layers in zirconolite and pyrochlore; the stacking vector SV and the stacking angle SA (8). For zirconolite-2M, Fig. 2, the repeat sequence is represented by the stacking vector SV connecting points A and B, and then B and C with the crystallographic repeat defined by starting and finishing on *c-centered points*. For a perfect HTB motif the stacking angle SA is 60°. In the present definition both SV and SA are independent of the atomic coordinates and can be expressed in terms of the lattice parameters as described in Table 1 and Fig. 3. Adjacent HTB layers in zirconolite-3T and pyrochlore exhibit perfect hexagonal symmetry resulting in a SA of exactly 60°. An additional term that can be used to describe the stacking of layers is that of *modules*. A module consists of two adjacent HTB-type layers and the intervening Ca/Zr layer; thus adjacent modules consist of three HTB layers and the two intervening Ca/Zr layers.

SAMPLE PREPARATION AND ANALYTICAL PROCEDURES

Fabricating near Single-Phase 4M Specimens

It is difficult to fabricate single-phase Nd-substituted zirconolite samples because exact compositions that form at Nd levels between 0.5 and 0.8 ions per formula unit have not been previously identified. We have therefore carried out a systematic analysis with differing proportions of starting materials to identify the conditions leading to single-phase zirconolites. With the procedure adopted it is possible to control the impurity phases so that perovskite is the only

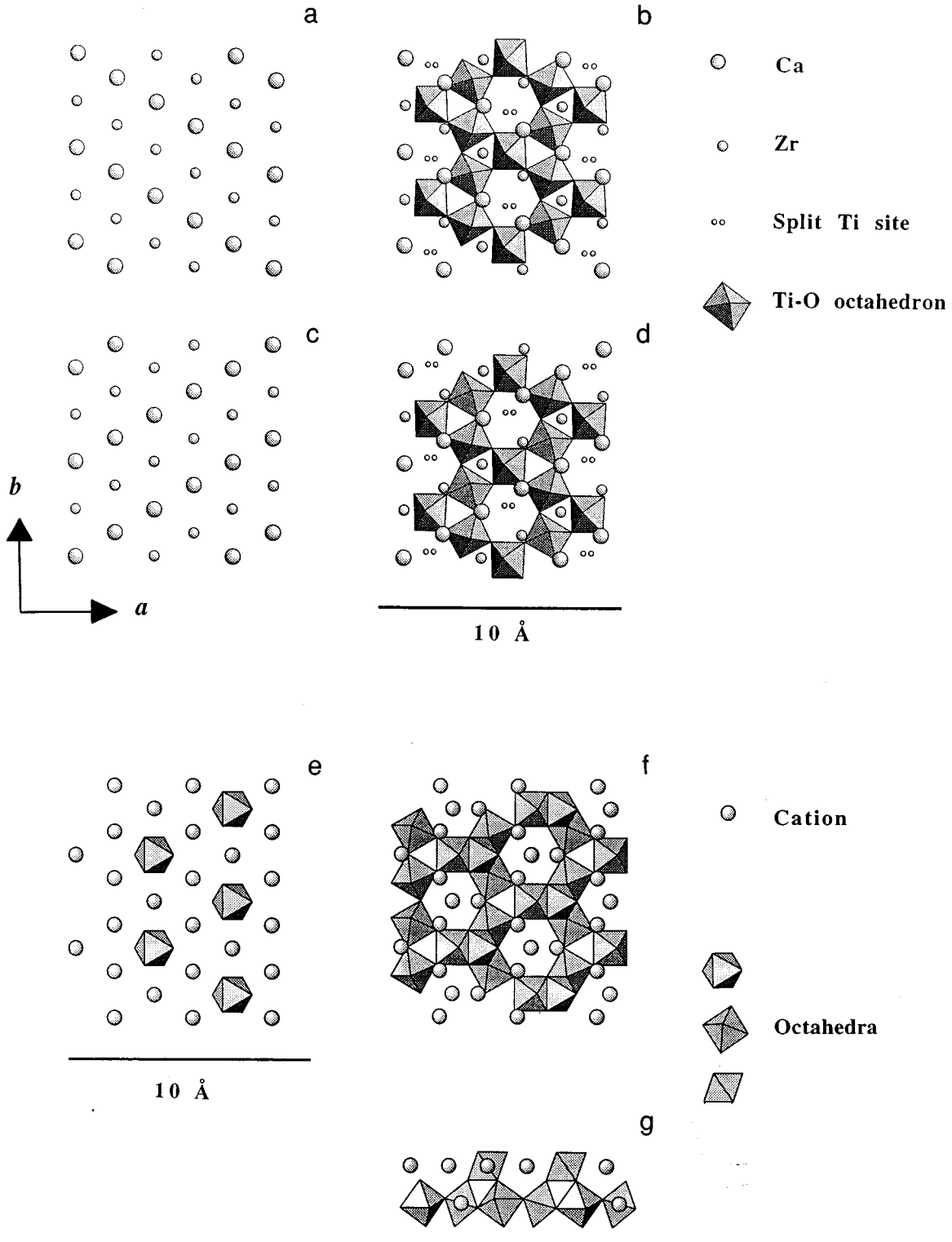

FIG. 1. Slices through the crystal structures of zirconolite (a–d) and pyrochlore (e–g) drawn using data from Gatehouse *et al.* (9) and Chakoumakos (5) respectively. Octahedra represent cations surrounded by anions. Apicies indicate anion positions. (a–d) show sections of zirconolite parallel to (001). (b) $0.0 \leq z \leq \sim 0.5$. (d) $0.0 \leq z \leq \sim 1.0$. (e–g) show sections of pyrochlore parallel to (111). (011) is vertical in (e, f). (g) is a bottom view of (f); i.e., (g) is (f) rotated by 90° around a horizontal axis in the plane of the page. Both zirconolite and pyrochlore contain layers primarily composed of octahedrally coordinated cations. (b, d, f) show the relative orientation of layers containing octahedra and the cation layers which lie directly above them (a, c, e) show only the layers of cations which lie above layers containing octahedra.

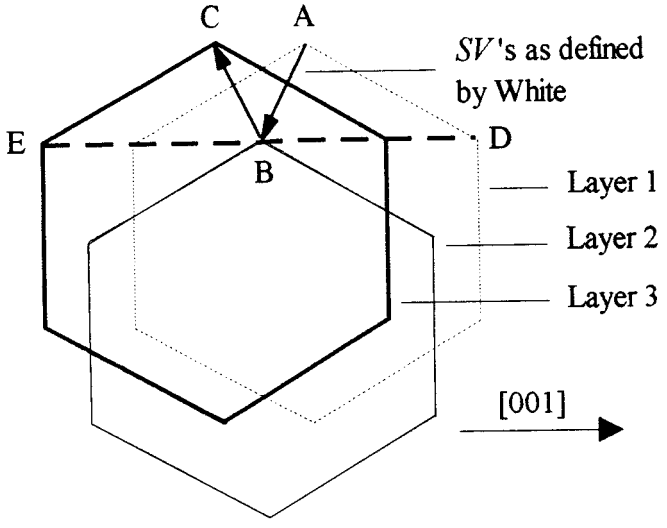

FIG. 2. Stacking vector as defined by White (8). The nodes of the hexagonal rings represent the Ti(1) and Ti(3) sites of the HTB layers. Points *A*, *B*, and *C* represent Ti(3) site projections down **c*** onto the (001) plane. For perfect hexagonal symmetry, point *B* would lie on the line connecting points *E* and *D*.

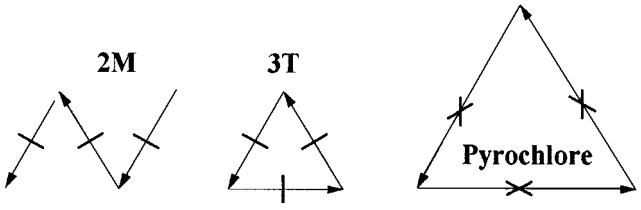

FIG. 3. Stacking vectors for the zirconolite-2M, zirconolite-3T, and pyrochlore structures. For the 2M and 3T cases, the short lines at the centers of the SVs indicate the directions of the Ca and Zr rows which lie between adjacent HTB layers represented by the vectors. For 3T and pyrochlore, the angle between successive vectors is exactly 60° and for zirconolite it is approximately 60°.

phase formed alongside the zirconolite. By investigating the relative concentration of these two phases in an X-ray powder pattern, an extrapolation technique has been developed to pinpoint the actual composition of the zirconolite phase formed.

In zirconolite, Nd^{3+} is expected to occupy either the Ca site or the Zr site (8, 11). Normally the substitution of Nd ions on to these sites requires the use of a compensating 3+ ion on the Ti sites to maintain charge neutrality within the structure and full occupancy of the sites, viz.,

$$[Ca_{1-x}Nd_x][Zr_{1-y}Nd_y][M^{3+}_{x-y}(Ti/Zr)^{4+}_{2-x+y}]O_7,$$

where M^{3+} is the compensating ion and $x \geq y$. Clearly if $x = y$ there is no need to use a compensating ion, but in practice Nd does not substitute in this way. Charge neutrality in Nd-substituted zirconolites can also be achieved by sacrificing the full occupancy constraint on the Ca and Zr sites. In the present work we have adopted the latter strategy in order to identify the manner and extent to which the zirconolite structure accommodates vacant cation sites. Without the inclusion of a compensating ion, the composition of a zirconolite with x Nd ions per cell is expected to fall somewhere between two extreme cases:

Case A: All Nd^{3+} on the Ca sites,

$$[Ca_{1-3x/2}Nd_x \otimes_{x/2}]ZrTi_2O_7,$$

where $\otimes$ represents a vacant site.

Case B: Nd^{3+} distributed equally on Zr and Ca sites,

$$[Ca_{1-x/2}Nd_{x/2}][Zr_{1-x/2}Nd_{x/2}]Ti_2O_7.$$

When samples with $x \approx 0.5$ to 0.8 are made up according to case A, a zirconolite phase forms but ZrO_2, TiO_2, and $ZrTiO_4$ also form as impurity phases. Conversely, when samples are made up according to case B, then the perovskite $[Ca, Nd]TiO_3$ is the only impurity phase. The perovskite $CaZrO_3$ or $(Ca[Ti_xZr_{1-x}]O_3)$, for any significant value of x, was not observed. The actual zirconolites that form invariably contain vacant sites where the Nd is partitioned unequally on the Ca and Zr sites with $Nd_{Ca} > Nd_{Zr}$ using the notation $occupancy_{\text{crystal site}}$.

Figure 4 shows the change in the X-ray diffraction pattern in a series of samples prepared with a range of intended vacancy concentrations and for an intended Nd/Ca ratio of 1.2. Extrapolating the intensity of the main perovskite peak to zero with respect to the cation molar proportions of Zr gives the composition of the zirconolite phase formed. The zirconolite phase compositions for starting materials which produce perovskite as the only impurity can also be determined using a modified form of the Rietveld method (7, 16) for quantitative phase analysis.

TABLE 1

Stacking Vectors (SVs) and Stacking Angles (SAs) for the Zirconolite-2M and -3T Polytypes and for Pyrochlore in Terms of Their Corresponding *a* and *b* Lattice Parameters

2M	$SA = 180 - 2\,\text{Arctan}\left(\frac{3b}{a}\right)$	$SV = \left\lvert\frac{c\cos(\beta)}{2\sin(SA/2)}\right\rvert$
3T	$SA = 60°$	$SV = \frac{a}{2\sqrt{3}}$
Pyrochlore	$SA = 60°$	$SV = \frac{a}{\sqrt{6}}$

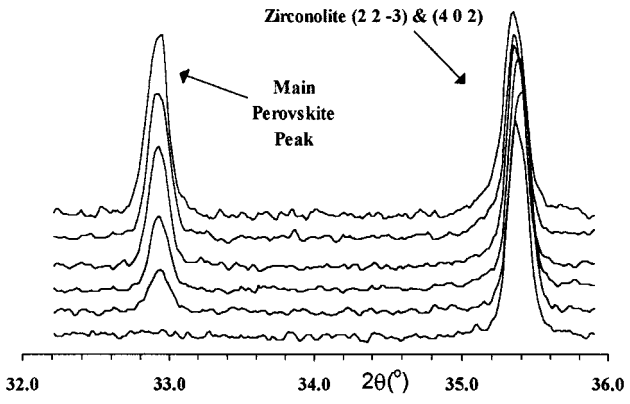

FIG. 4. XRD patterns of Nd-doped zirconolite-4M using Cu$K\alpha$, showing the reduction in intensity of the main perovskite peak with increasing intended vacancy concentration.

As a consistency check on the above results, samples with low and high intended vacancy concentrations were analyzed at ANSTO by Dr. Arthur Day using backscatter imaging and X-ray microprobe analysis on a scanning electron microscope (SEM). This work confirmed that starting mixtures which were formulated to yield low vacancy concentration zirconolites contained perovskite as the only impurity. At the other end of the scale, starting mixtures which were formulated to yield high vacancy concentration zirconolites contained TiO_2, ZrO_2, and $ZrTiO_4$ impurities. The formation of the impurity $ZrTiO_4$, in nontrivial quantities, was initially observed in the SEM. According to the structure of $ZrTiO_4$ (17), its main diffraction peak overlaps the strongest peak of zirconolite for Cu$K\alpha$. This was validated using high resolution XRD which separated the lattice peaks of zirconolite and $ZrTiO_4$.

Sample Preparation

All Nd-substituted samples were prepared by solid state reaction of predried Analar grade $CaCO_3$, Nd_2O_3, TiO_2, and ZrO_2 between 1380°C and 1400°C for 12 hrs following a thorough mixing and prefiring stage. As these materials tend to absorb differing proportions of moisture, especially Nd_2O_3 which can increase its weight by up to 15% wt. due to atmospheric moisture (7), all of the weighing out was closely coupled with the drying procedure to minimize the absorption time. Before preparing the samples, an investigation was carried out to develop a simple but effective mixing procedure to obtain homogeneous specimens. Sample inhomogeneity is readily identified in XRD patterns as line broadening of diffraction peaks arising from variations in composition within the specimen. After investigating a number of approaches, we have adopted a wet mixing procedure using a high speed (18,000 RPM) blade mixer in an enclosed chamber with petroleum spirit as the mixing fluid. We have found that the diffraction patterns from specimens mixed in this way are invariably better resolved than specimens prepared either manually or by ball milling with other solvents. Petroleum spirit has a much lower viscosity than many common solvents so that large and small particles of different compounds do not fractionate in the mixing crucible as often happens with ethanol or acetone. Petroleum spirit is also easily recovered and can be reused without cross-contamination.

X-ray and Neutron Data Collection

The X-ray data used for quantitative analysis were collected using a conventional horizontal powder diffractometer of radius 205 mm fitted with a long fine focus Cu X-ray tube set at 35 kV and 45 mA. The system was equipped with a Ge premonochromator set for Cu$K\alpha_1$ radiation and a position sensitive detector (PSD). Excellent counting statistics were obtained with 40,000 counts on the main zirconolite peak. The rocking curve effect achieved by step scanning the PSD (18) gave smooth diffraction patterns because of the increased number of crystallites sampled for the diffraction pattern relative to a standard powder pattern. Each diffraction sample was ground to a fine powder and side loaded into a sample holder recess to present a smooth flat surface to the incident X-ray beam. The crystallite size of all the specimens was $\sim 1\ \mu m$, and the X-ray pattern recorded displayed no signs of irregularities arising from crystallite size statistics. All the X-ray patterns were recorded with a step size of $0.01^\circ\ 2\theta$ over an angular range from 13° to $120^\circ\ 2\theta$. Neutron diffraction data were collected using the high resolution powder diffractometer (19) at the Lucas Heights HIFAR reactor with $\lambda = 1.4925$ Å.

Both the X-ray and neutron data were analyzed by the Rietveld method (20, 21). The actual refinement program used for analysis (7) was developed at UTS to accommodate some of the specific problems associated with the current investigation. Its unique features include the automatic generation of *hkl*'s and multiplicities which makes it possible to assign a set of equivalent positions to a site without knowing the space group of the structure, and the inclusion of chemical constraints to help improve the accuracy of the quantitative analysis of both the weight fractions of formed impurity phases and the chemical compositions of the zirconolite actually prepared.

Electron Microscopy

High resolution transmission electron microscopy (HRTEM) and selected area diffraction (SAD) were performed using a JEOL 2000FX transmission electron microscope operated at 200 KV.

RESULTS

2M Model Analysis

The 2M structural model as described by Gatehouse *et al.* (9) was used as a starting model in the present analysis. Data from two series of samples, one series at the low end of the solid solution limit and another at the high end of the solid solution limit, were analyzed to identify and prepare two single-phase 4M specimens. Compositions determined using the extrapolation based technique were

$$\begin{aligned} &Ca_{0.699}Nd_{0.517}Zr_{0.763}Ti_2O_7,\ \otimes = 0.021\ \text{(A)} \\ &Ca_{0.564}Nd_{0.677}Zr_{0.710}Ti_2O_7,\ \otimes = 0.049\ \text{(B)}. \end{aligned} \quad (1)$$

They correspond to single-phase 4M for Ti = 2 close to the lower and upper compositions of the 4M solid solution range. The compositions of Eq. [1] were used as a guide for fabricating a further five 4M samples including two large 20-g samples for neutron diffraction. These samples all contained zirconolite-4M as the primary phase and small quantities of the perovskite $[Ca_{1-3x/2}Nd_x]TiO_3$. Owing to the perovskite impurity, the composition of the 4M phase formed was slightly different from the intended composition. In this analysis the actual compositions were derived from fitting the X-ray diffraction data using a version of Rietveld refinement (7) incorporating chemical constraints based on the composition of the starting materials, and that the zirconolite formed is electrostatically neutral. The compositions of the present 4M specimens determined in this manner are shown in Table 2. A near linear relationship for Nd concentration versus total (Zr + Ti) content is observed which indicates the substitutional equivalence of Zr^{4+} and Ti^{4+} atoms. The Nd solid solution limits for Ti = 2 were identified as

$$0.49(1) < \text{Nd per 2M formula unit} < 0.80(1).$$

It was found that Rietveld refinement of the above samples gave similar scattering amplitudes on the Ca and Zr sites over the Nd solid solution range. This suggests that the cation distribution amongst these sites is one of a random distribution of Ca^{2+}, Nd^{3+}, Zr^{4+}, and Ti^{4+} atoms, which means that a large percentage of the Ca site would be occupied by small Zr^{4+} atoms. The result is consistent with the idea that the Ca and Zr sites of 4M are not coincident with 2M Ca and Zr sites.

X-ray and neutron data for samples 1 and 5 of Table 2, corresponding to the upper and lower Nd limits, were collected, and structural refinement was carried out to determine the fractional atomic coordinates and cation site occupancies, using a 2M structural model. The fits to the neutron patterns were generally poor ($R_{wp} \cong 15\%$) and discrepancies could not be accounted for using the 2M model. When the structural data were compared to the Gatehouse *et al.* (9) data for nominal zirconolite, relatively large differences between the oxygen x and y fractional atomic coordinates were observed with only small differences in the z coordinates. The conclusion is that the HTB layers in the 4M structure stack in a similar manner to zirconolite-2M in the **c*** direction but undergo translations in the **a**–**b** plane relative to the 2M model.

Rietveld fits to the X-ray diffraction patterns using the 2M model were good except that it was not possible to account for low angle diffraction peaks with d-spacing corresponding to (001) and (003) peaks of relatively low intensity. These reflections are absent in $C2/c$ and indicate the inadequacy of the 2M model in describing zirconolite-4M. However, since the X-ray data and, to a limited extent, the neutron data fit moderately well, it was obvious that the 4M model would be similar to 2M. In particular, individual HTB layers were expected to be very similar to those of the 2M model and not modified as in, for example, the orthorhombic polymignyte structure described by White (8). Also since the fits to the X-ray data were good, it was expected that the 4M cation positions would be similar to the 2M model.

TABLE 2
4M Phase Compositions and Lattice Parameters Determined for Samples 1 to 5

Sample	Ca	Nd	Zr	Ti	⊗	*a* (Å)	*b* (Å)	*c* (Å)	*β* (°)	SA(°)
1[a]	0.721	0.494	0.772	1.997	0.016	12.522	7.222	11.634	100.32	60.05
A	**0.699**	**0.517**	**0.763**	**2**	**0.021**					
2	0.687	0.521	0.768	1.997	0.026	12.544	7.233	11.645	100.30	6.006
3	0.573	0.659	0.733	1.986	0.049	12.545	7.245	11.666	100.32	59.99
B	**0.564**	**0.677**	**0.710**	**2**	**0.049**					
4	0.531	0.703	0.716	1.991	0.059	12.553	7.248	11.665	100.32	60.00
5[a]	0.479	0.760	0.716	1.975	0.071	12.553	7.248	11.681	100.30	60.00

Note. Samples labeled A and B corresponds to the extrapolation compositions of Eq. [1].
[a] Samples 1 and 5 are large 20-g samples for neutron diffraction.

HRTEM and SAD of sample 1 shows that it has a layer structure and that most of the sample has a repeat spacing of $\sim$23 Å. The pairs of photos in Fig. 5 reflect the range of perfection seen in this sample. Some areas are nearly perfect (Figs. 5a and 5b), while others contain large slabs with spacings other than $\sim$23 Å (Figs. 5c and 5d).

The lattice parameters obtained by refinement for the five 4M samples are shown in Table 2. The stacking angles, the angle between stacking vectors, of $\sim$60.0°, indicate almost perfect hexagonal symmetry in the **a**–**b** plane. It seems therefore that the symmetry in the **a**–**b** plane is closely related to the hexagonal symmetry of pyrochlore.

Determination of the Zirconolite-4M Structure

Based on the insight given by the 2M analyses, an approach was adopted in which individual zirconolite HTB layers were stacked in different ways to develop a model that fitted both the X-ray and neutron diffraction data. To simplify the process it was assumed that only stacking vectors applicable to zirconolite and pyrochlore are permissible. This seems reasonable based on the 2M analysis above, and the fact that the 4M structure is observed for Nd concentrations between that of zirconolite-2M and pyrochlore. The reasonable fits to the X-ray data also indicate that the cation positions are similar to either zirconolite-2M or pyrochlore positions.

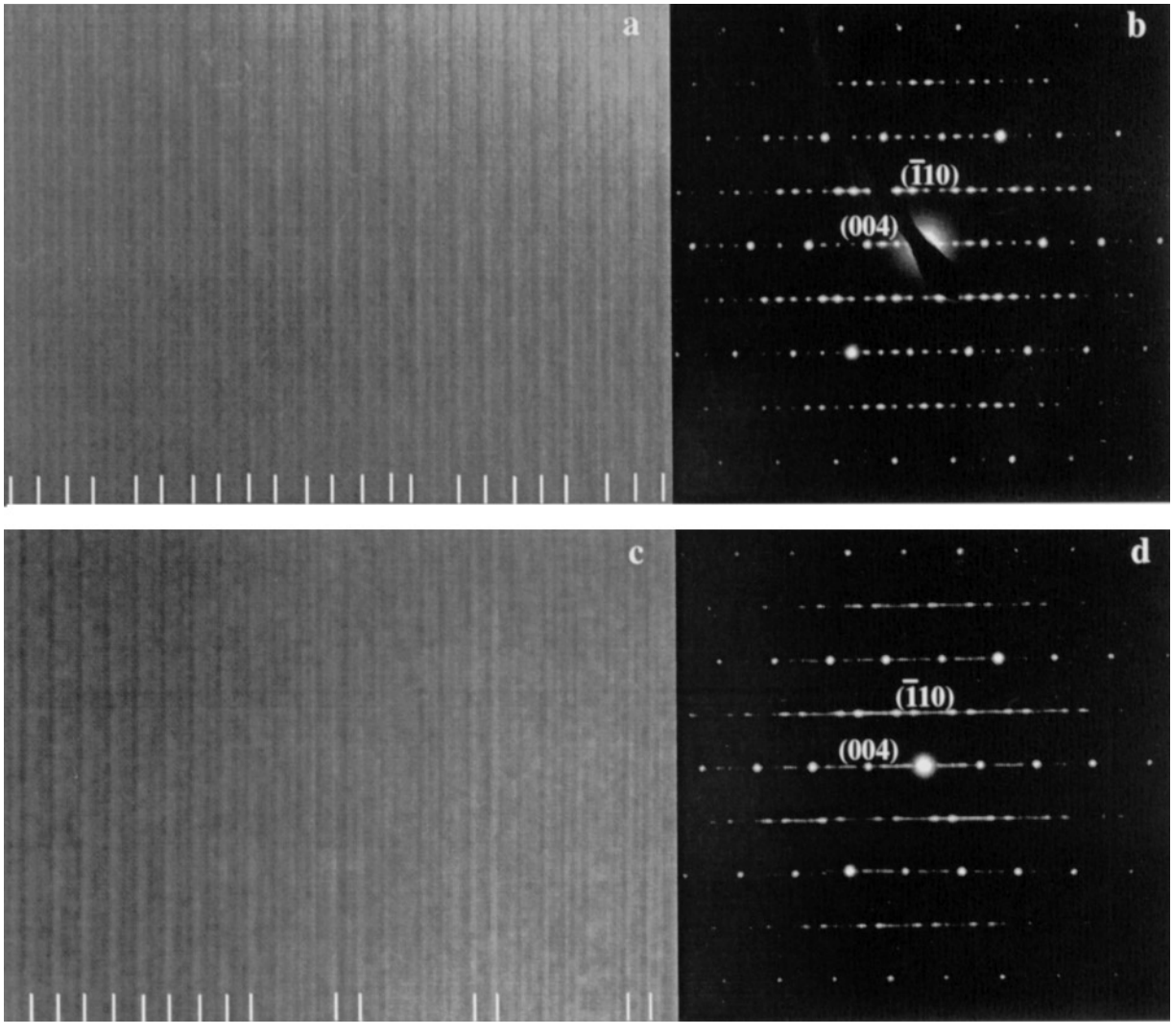

FIG. 5. Pairs of HRTEM images and SAD patterns of parts of grains of Sample 1. The distances between the white markers indicate a $\sim$23-Å crystallographic repeat along z. (a) An area of crystal containing only three defects. (b) SAD pattern of (a). (c) A relatively imperfect area of crystal. (d) SAD pattern of (c) showing streaking symptomatic of the variety of layer widths. (a, c) are 550 Å wide. The labeled reflections in (b, d) are those which lie directly below the central figure of their label.

The two interlayer cation sites, Ca and Zr sites, were both initially fixed to their nominal 2M positions and given a single-site occupancy parameter that was refined in each of the different HTB stacking sequences trialed. Although the unit cells of the various HTB configurations are dependent upon the stacking vectors, a monoclinic *c*-centered cell was assumed with *a* and *b* lattice parameters similar to the 2M model. Only stacking vector configurations consistent with this model were considered.

The fractional atomic coordinates for an individual HTB layer in zirconolite-2M can be isolated from the $C2/c$ description. Changing the z equivalent positions to reflect a four-layered structure, the equivalent positions of a single zirconolite HTB layer with the center of the hexagonal ring as the origin are as shown in Table 3a. Table 3b shows the coordinates of the anions and cations in the first HTB layer which is referred to as HTB(0). More generally HTB(n) indicates a layer which is a translation of HTB(0) according to the possible stacking vectors defining the relative positions of the layers.

In building a 4M model, the first HTB layer and associated cations are given the same orientation as the first layer of the 2M model. This means that there can only be three possible zirconolite-type stacking vectors as shown in Fig. 6 with the first stacking vector labeled (1). Only three possibilities are considered so that the center of an HTB layer is not positioned directly above an interlayer cation. Also, there are only three possible pyrochlore-type stacking vectors as shown in Fig. 6. By connecting the stacking vectors of Fig. 6 head to tail to form a four-layer repeat sequence, with the constraint that the unit cell of the result must be monoclinic, seven stacking sequences were identified as illustrated in Fig. 7.

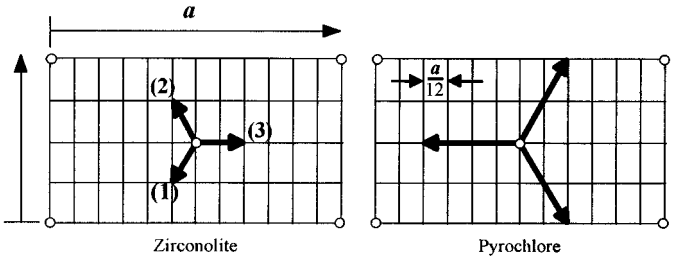

FIG. 6. Possible zirconolite and pyrochlore stacking vectors. The vector labelled (1) is chosen as the first stacking vector and corresponds to the first zirconolite module. **a** and **b** corresponds to the lattice vectors in the 2M model. The grid spacing is determined from considering perfect hexagonal symmetry. The three pyrochlore vectors shown all translate to identical surroundings and are therefore equivalent.

The unit cells for the sequences of Fig. 7 can all be expressed in terms of the 2M lattice vectors. In each case the supercell is monoclinic with the **a** and **b** vectors identical to the 2M model. With subscripts "2M" and "4M" for 2M and four-layered models respectively, we have for models 7a to 7d $\mathbf{c}_{4M} = 2\mathbf{c}_{2M}$ and $\beta_{4M} = \beta_{2M}$, and for models 7e to 7g $\mathbf{c}_{4M}$ and β_{4M}. For models 7f and 7g, β_{4M} could be made

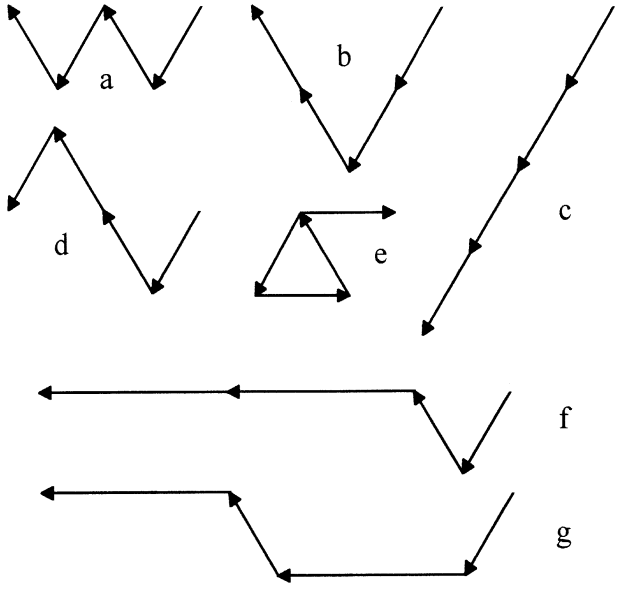

FIG. 7. Possible stacking vector sequences for a four-layered monoclinic unit cell. Projections are made down **c***. Short and long vectors correspond to zirconolite and pyrochlore modules, respectively. Note a module consists of two consecutive HTB layers. Model (a) corresponds to the nominal 2M model.

TABLE 3

(a) Symmetry-related Coordinates for Each Site in the First HTB Layer of the 4M Structure, and (b) Fractional Atomic Coordinates for the Sites in the First HTB Layer (HTB(0)) in the 4M Structure

(a) Symmetry-related coordinates	(b) Site	x	y	z
$x, y, 0.125 + z$	T (1)	0.2526	0.2547	−0.0016
$-x, y, 0.125 - z$	T (2)	−0.0300	−0.0520	0.0063
$0.5 + x, 0.5 + y, 0.125 + z$	T (3)	0.0000	0.5000	0.0000
$0.5 - x, 0.5 + y, 0.125 - z$	O (1)	0.1810	0.0049	−0.0129
	O (2)	−0.0065	0.0140	0.0794
	O (3)	0.2536	0.2145	0.0852
	O (4)	0.0941	−0.3014	0.0197
	O (5)	0.2510	0.2858	−0.0867
	O (6)	−0.0521	0.5076	0.0812
	O (7)	0.1028	0.3208	0.0125

Note. For each site four symmetry-related coordinates are generated from the equivalent positions of (a).

equivalent to β_{2M} by doubling $\mathbf{c}_{4M}$. This is because after eight HTB layers, models 7a, 7f, and 7g are all translated the same distance in the **a** direction.

Each possible 4M structure can be found by translating the HTB layer in the **a**–**b** plane (i.e., HTB(0)) to the positions at the start (or end) of the stacking vectors. The translation in the **c*** direction is given by $nc^*/4$ where n corresponds to the HTB number. The interlayer cations in these models are set to their nominal positions. Simultaneous refinements using the neutron and X-ray data with all the oxygen fractional coordinates refined gave poor fits to all models except model 7g. This refined to an R_{wp} of 9.3% where as the next best fit, model 7a refined down to an R_{wp} of 15.5%. The visual improvement in the fit and the fact that the (002) and (006) lines was evident was very encouraging.

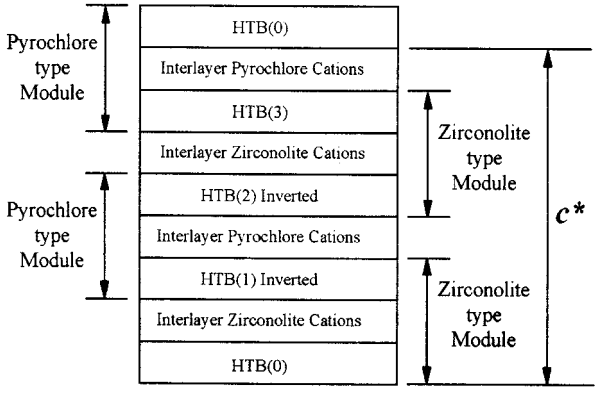

FIG. 8. Schematic of the zirconolite-4M structure.

Further Refinements to the Structure

Model 7a. The stacking of the HTB layers has thus far consisted of translations of HTB(0) in the **a**–**b** plane and in the **c*** direction. In the 2M model, as described by the space group $C2/c$, HTB layers are related by an inversion and a translation. To incorporate an inversion in the present 4M model for model 7a, HTB(0) is inverted for layers 1 and 3 before translating to the HTB(1) and HTB(3) positions. On subsequent refinement, an R_{wp} of 14.9% was obtained for model 7a, a value identical to that obtained using the standard 2M unit cell. Thus the HTB layers of a zirconolite module (short stacking vectors) are related by an inversion and a translation.

Model 7g. The HTB layers of nominal pyrochlore are related only by a translation and no inversion (7). To have the HTB layers of the zirconolite modules of model 7g related by an inversion and a translation, and the HTB layers of the pyrochlore-like modules related only by a translation, we invert HTB(1) and HTB(2) before translation. After refinement an R_{wp} of 8.9% is obtained. From the stacking vectors and the inversions, the following symmetry related coordinates are obtained for each site:

$$(0, 0, 0; \tfrac{7}{8}, \tfrac{1}{2}, \tfrac{3}{4}) + \text{HTB(0) and } (\tfrac{7}{8}, \tfrac{3}{4}, \tfrac{1}{4}; 0, \tfrac{1}{4}, \tfrac{1}{2}) + \text{HTB(0) Inverted.} \quad [2]$$

These describe a structure of alternate zirconolite and pyrochlore-type modules as illustrated in Fig. 8. Each HTB layer is sandwiched between interlayer zirconolite and pyrochlore cations and has identical surroundings. Interlayer zirconolite cations consist of Ca and Zr sites, and interlayer pyrochlore cations consist of Ca and Ti sites. From studies on nominal zirconolite and pyrochlore it is known that zirconolite modules are compressed relative to pyrochlore modules. This is expected since the average size of the interlayer zirconolite cations is less than those of pyrochlore. To account for possible compression of the zirconolite-type modules, or expansion of the pyrochlore type modules, the HTB layers must be given a degree of freedom in the **c*** direction. The only way of doing this is to split the 16 equivalent positions of Eq. [2] into two groups as shown in Table 4. This doubles the number of sites, one site for group 1 positions and another for group 2 positions. This greatly increases correlation amongst the parameters during refinement. To overcome this, the sum of any two parameters between the groups are constrained to double that of the original value. This assumes that the original value at $R_{wp} = 8.9\%$ represent the true average value. On incorporation of these changes the R_{wp} dropped to 8.2% after subsequent refinement.

Inspecting the interlayer cation sites, it is found that they can all be described using either group (1) or (2) positions of Table 4, with a total of three Ca sites, one Zr site, and one Ti site. Assigning an occupancy parameter to each of these and then refining, the R_{wp} dropped to 7.8%. It is worth noting that this value is typical of fits obtained for well-crystallized zirconolite-2M (7). Figure 9 shows the fit obtained for the low angle (002) peak for the X-ray data of sample 1 with

TABLE 4
Equivalent Positions of Eq. [2] Split into Two Groups Allowing the HTB Layers to Move Independently

Group 1 positions, (0, 0, 0; 0.5, 0.5, 0)			Group 2 positions, (0, 0, 0; 0.5, 0.5, 0)		
x	y	$0.125+z$	$-x$	y	$0.125-z$
$0.375-x$	$0.25-y$	$0.375-z$	$0.375+x$	$0.250-y$	$0.375-z$
x	$0.25-y$	$0.625+z$	$-x$	$0.250-y$	$0.625-z$
$0.375-x$	y	$0.875-z$	$0.375+x$	y	$0.875+z$

Note. The two groups can be made equivalent with x(group 1) = $-x$(group 2) and z(group 1) = $-z$(group 2).

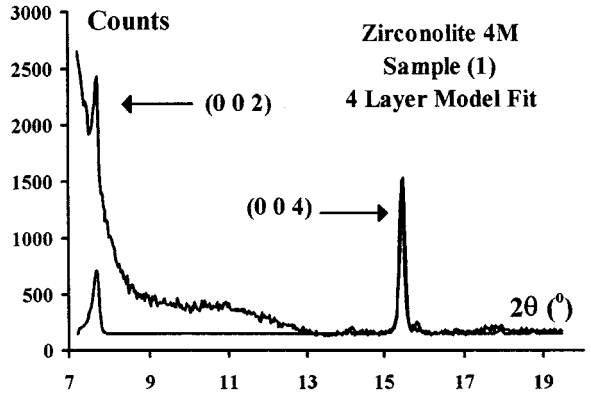

FIG. 9. Observed and calculated low angle (002) peak generated using the 4M model for sample 1 and Cu$K\alpha$ radiation.

Cu$K\alpha$ radiation. This peak is forbidden in the 2M model and is an indication of the validity of the present 4M model.

Structural Data and Space Group Determination—C2/c

In total, the 4M model consist of 24 sites each with equivalent positions described by either group (1) or group (2) positions of Table 4. These positions can be described by the $C2/c$ space group as given in Table 5. The terminology adopted uses a "Z" (as in Ca(Z)) to represent the cation sites of the zirconolite module, and a (P) (as in Ca(Pn)) to represent the cation sites of the pyrochlore-type module. A schematic of the structure is shown in Fig. 10. The layers at $z = \sim 0.25$ and ~ 0.75 are similar to cation layers in pyrochlore. The layers at $z = \sim 0.50$ and ~ 1.00 are similar to cation layers in zirconolite-2M. The layers containing octahedrally coordinated cations also contain split Ti sites and are consequently similar to those in zirconolite and dissimilar to those in pyrochlore.

Since the sites requiring equivalent positions of both groups 1 and 2 were not refined independently, the fractional atomic coordinates of only one site is given; these are superscripted with a "1". The means of generating the second site is given in Table 5. It is anticipated that data of higher resolution and better counting statistics, single-crystal data for example, would allow for a full and accurate refinement.

The interfacial angles and bond lengths of the Ti(1) and Ti(3) octahedra of the present model are similar to that of the zirconolite-2M structure as determined by Gatehouse *et al.* (9). This is reassuring since Ti octahedra across different structures are expected to be similar. The Ti(P) octahedra, however, show distortions, which could be due to a large amount of Zr^{4+} substitution in that site or the fact that the two sites required for each ^{1}O1(n) were not refined independently. The site occupancy analysis presented below does in fact show a large amount of Zr^{4+} in the Ti(P) site.

Further support is given by the magnitude of the observed **c*** lattice parameter of the 4M structure which is between the nominal zirconolite and pyrochlore values. The **c*** per layer for zirconolite and pyrochlore given by Mazzi and Munno (14) are 5.627 and 5.947 Å, respectively. From Table 5, the **c*** per layer observed for the present 4M samples range from 5.723 Å for sample 1 to 5.746 Å for sample 5.

It is also interesting to note the minimum number of Nd^{3+} ions required to make up an electrically neutral 4M unit cell consists of 20 Ca positions, 8 Zr positions, 36 Ti positions, and 112 O positions. If each position is occupied by its nominal cation then there would be a positive ionic charge of 216 and a negative ionic charge of -224. Assuming Nd^{3+} ions substitute for Ca^{2+} ions only, the minimum amount of Nd^{3+} required for charge balance can be calculated by solving the two equations $Ca + Nd = 20$ and $2\ Ca + 3\ Nd = 48$. From this we get $8\ Nd^{3+}$ ions and $12\ Ca^{2+}$ ions per unit cell. Converting this to a zirconolite-2M composition gives the nominal chemical equation of $[Ca_{0.75}Nd_{0.5}]Zr_{0.5}Ti_{2.25}O_7$. This composition is almost exactly that found at the low end of the solid solution range determined earlier. Also the total Ca + Nd content as determined throughout the solid solution range in the current analysis, Table 2, range from 1.22 to 1.24 which is similar to the expected value of 1.25.

An interesting aspect of the 4M chemical formula is the total Zr/Ti ratio of 0.22 for nominal 4M. This value is considerably less than the value of ~ 0.375 for the samples fabricated in the current analysis. Because of this a large amount of Zr ions would be required to fill the Ti sites and presumably affect the stability of the structure. Further investigation into the effect this ratio has on the structure is recommended.

Site Occupancy Analysis Using the 4M Model

A site occupancy analysis was carried out on two 4M specimens near the solid solution limits using the structural parameters of Table 5 and X-ray diffraction data. Results should reflect expected cation distributions amongst the cation sites. Step-scanned X-ray diffraction patterns in the range 12° to 120° 2θ were collected using Cu$K\alpha$ radiation. The samples were rotated in order to minimize on preferred orientation effects. Phase compositions were determined using the chemical constraint that the relative proportions of the cations in the fired product are the same as the starting mixture before firing, and that the zirconolite formed is ionic and electrostatically neutral. Converted to 14 oxygens (2×2M unit cell), the compositions for the 4M phases for the two samples, samples 1 and 6, are shown in Table 6 (Row A). These compositions should be reflected in

TABLE 5
Structural Parameters Determined from Rietveld Refinement for Samples 1 and 5 of Table 2

Structural parameters for Zirconolite-4M, space group $C2/c$
Number of sites per 7 oxygen sites
1.25 Ca sites, 0.5 Zr site, 2.25 Ti sites, 7 O sites

	Sample 1			Sample 5		
	$Ca_{0.721}Nd_{0.494}Zr_{0.772}Ti_{1.997}O_7$, $\square = 0.016$			$Ca_{0.479}Nd_{0.760}Zr_{0.716}Ti_{1.976}O_7$, $\square = 0.071$		
	$a = 12.522(2)$ Å			$a = 12.553(2)$ Å		
	$b = 7.222(2)$ Å			$b = 7.248(2)$ Å		
	$c = 22.987(2)$ Å			$c = 23.081(2)$ Å		
	$\beta = 84.791(5)^\circ$			$\beta = 84.799(5)^\circ$		
	Interlayer Pyrochlore cations. Ca(P1) and Ti(P) are (4e) sites					
Ca(P1)	0	0.1246	0.25	0	0.1252	0.25
Ca(P2)	0.7529	0.8734	0.2508	0.7514	0.8853	0.2488
Ti(P)	0	0.6287	0.25	0	0.6291	0.25
	Interlayer Zirconolite cations					
Ca(Z)	0.8751	0.3777	0.4931	0.8755	0.3726	0.5045
Zr	0.8738	0.8765	0.4989	0.8711	0.8638	0.4945
	HTB sites					
Ti1(1)[a]	0.0640	0.8842	0.3786	0.0630	0.8831	0.3759
Ti1(2)[a]	0.7838	0.1359	0.3797	0.7825	0.1770	0.3813
Ti(3)	0.8032	0.6244	0.3764	0.8125	0.6250	0.3750
O1(1)[a]	1.0083(26)	0.1210(58)	0.3625(12)	0.9953(27)	0.1281(59)	0.3611(13)
O1(2)[a]	0.8040(31)	0.1126(65)	0.4539(11)	0.8033(31)	0.1153(66)	0.4548(12)
O1(3)[a]	0.0619(38)	0.9067(58)	0.4596(13)	0.0629(36)	0.9027(61)	0.4598(14)
O1(4)[a]	0.9059(36)	0.4240(45)	0.3934(13)	0.9079(39)	0.4331(48)	0.3954(14)
O1(5)[a]	0.0639(39)	0.8350(55)	0.2901(15)	0.0591(40)	0.8381(56)	0.2906(17)
O1(6)[a]	0.7592(25)	0.6164(85)	0.4587(15)	0.7589(27)	0.6150(83)	0.4587(17)
O1(7)[a]	0.9095(39)	0.8180(47)	0.3890(14)	0.9092(37)	0.8046(47)	0.3883(15)

	Mean M–O bond lengths ± 0.02 (Å)		
	CN		
Ca(P1)	8	2.46	2.44
Ca(P2)	8	2.46	2.48
Ti(P)	6	1.95	1.96
Ca(Z)	8	2.46	2.45
Zr(Z)	7	2.24	2.25
Ti1(1)[a]	6	1.97	2.00
Ti1(2)[a]	5	2.12	2.08
Ti(3)	6	1.94	1.91

[a] Two sites need to be generated for each of these sites, one where the coordinates are as stated and another with coordinates of $x \to x - \frac{5}{8}$, $y \to -y$, $z \to z + \frac{1}{4}$.

the composition obtained from the present site occupancy analysis. Any large deviations would bring into question the validity of the current 4M model. In the following Rietveld refinement of the site occupancies, the equivalent temperature parameters for all sites were fixed to the single value of 0.5 Å^2. The reason for this is strong correlations between the temperature parameters and site occupancies.

There are a total of 10 cation sites in the 4M structure and each may contain a number of site occupancies. Without meaningful constraints, refinement of all occupancy parameters leads to physically meaningless results. In a preliminary analysis the Ti(3) site occupancy refined to a value corresponding to full occupancy with Ti^{4+} atoms. With italic script to refer to an occupancy on a particular crystallographic site, given by the subscript $occupancy_{\text{crystal site}}$, the Ti(3) site occupancy was fixed to $Ti_{\text{Ti(3)}} = 1$ and the rest of the sites were assigned the following occupancies and constraints:

- The Ti1(1) and Ti2(1) sites were assigned equivalent occupancy parameters, and the sites were grouped into a

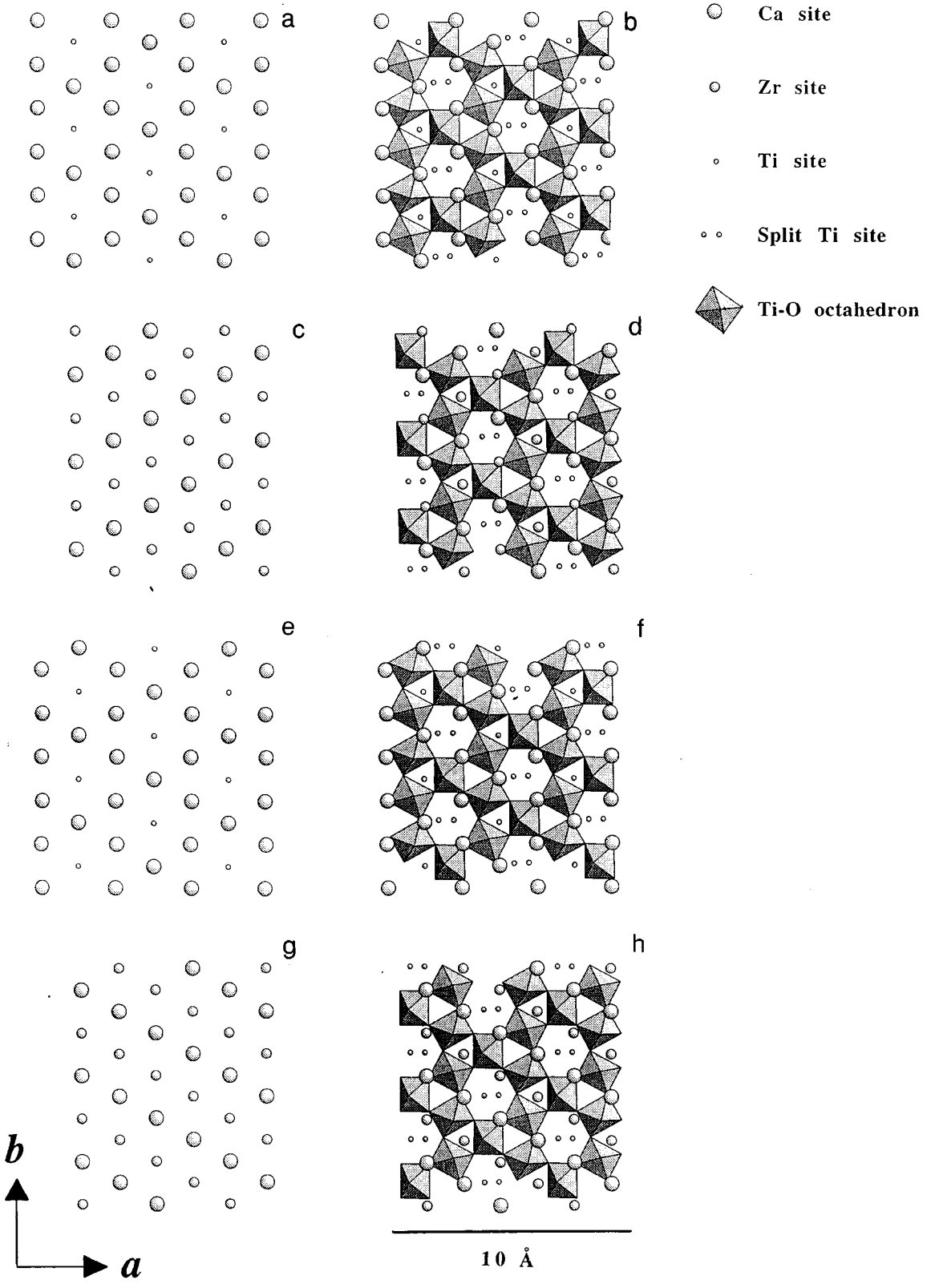

FIG. 10. (a–h) Sections through the crystal structure of zirconolite-4M parallel to (001). Octahedra represent cations surrounded by anions. Apicies indicate anion positions (a) $z = \sim 0.25$, (b) $0.0 \leq z \leq \sim 0.25$, (c) $z = \sim 0.5$, (d) $0.25 \leq z \leq \sim 0.50$, (e) $z = \sim 0.75$, (f) $0.50 \leq z \leq \sim 0.75$, (g) $z = \sim 1.0$, (h) $0.75 \leq z \leq \sim 1.0$. (b, d, f, h) show the relative orientation of layers containing octahedra and the cation layers which lie directly above them (a, c, e, g) show only the layers of cations which lie above layers containing octahedra.

TABLE 6
Zirconolite-4M Compositions Obtained Using Chemical Constraints (Row A) and Compositions Obtained without Chemical Constraints (Row B)

	Sample 1 of Table 2	Sample 6
Row A	$Ca_{1.44(1)}Nd_{0.99(1)}Zr_{1.54(1)}Ti_{3.99(1)}O_{14}$	$Ca_{1.14(1)}Nd_{1.38(1)}Zr_{1.40(1)}Ti_{4.00(1)}O_{14}$
Row B	$Ca_{1.48(7)}Nd_{0.99(7)}Zr_{1.47(8)}Ti_{4.03(8)}O_{14}$	$Ca_{1.30(7)}Nd_{1.12(7)}Zr_{1.44(7)}Ti_{4.06(7)}O_{14}$

single Ti(1) site. Similarly the Ti1(2) and Ti2(2) sites were grouped as the Ti(2) site.

- The Ca(Z) and Ti sites were constrained to full occupancy and vacancies were evenly distributed amongst the Ca sites.
- Ca and Nd ions occupy the Ca sites in various proportions.
- Zr and Ti ions occupy the Zr and Ti sites in various proportions.

These constraints allow for various proportions of Ca and Nd ions on the Ca sites, and Zr and Ti ions on the Zr and Ti sites. One limitation of the present model is the possibility of Nd ions on the Zr(Z) site and the possibility of Zr ions on the Ca sites. Results from refinement are shown in Table 7. All of the occupancies are positive, and furthermore the distribution of the Zr/Ti ions on the Zr(Z), Ti(1), and Ti(2) sites is consistent with the present 4M model, in that the sites are predominantly occupied by their corresponding nominal cations.

Most of the Zr ions are expected to reside on the Ti sites as the total Zr content (i.e., 1.54 and 1.40 for samples 1 and 6 respectively) is larger than the number of Zr positions (i.e., 1/cell). From the site occupancy results of Table 7 it seems that a large amount of Zr ions occupy the Ti(P) site. The values obtained though for $Zr_{Ti(P)}$, for both samples 1 and 6, seem too large. Further work will need to be carried out to investigate the effects of changing the Zr/Ti ratio for a fixed Nd content.

Compositions corresponding to the site occupancies of Table 7 are shown in Table 6 (Row B). The agreement with the results of Row A, which were obtained with chemical constraints imposed, are good considering the strong correlation between the site occupancies and the various assumptions made concerning the possible distributions of the cations.

TABLE 7
Zirconolite-4M Site Occupancy Results without Phase Composition Constraints

Site	Sam. 1	Sam. 6
$Ca_{Ca(P1)}$	0.41(3)	0.33(3)
$Nd_{Ca(P1)}$	0.09(3)	0.15(3)
$Ca_{Ca(P2)}$	0.69(4)	0.58(4)
$Nd_{Ca(P2)}$	0.30(4)	0.38(4)
$Zr_{Ti(P)}$	0.26(3)	0.32(3)
$Ti_{Ti(P)}$	0.24(3)	0.18(3)
$Ca_{Ca(Z)}$	0.38(4)	0.38(5)
$Nd_{Ca(Z)}$	0.61(4)	0.59(5)
$Zr_{Zr(Z)}$	0.92(2)	0.97(2)
$Ti_{Zr(Z)}$	0.08(2)	0.03(2)
$Zr_{Ti(1)}$	0.18(3)	0.12(2)
$Ti_{Ti(1)}$	0.82(3)	0.88(2)
$Zr_{Ti(2)}$	0.10(2)	0.01(2)
$Ti_{Ti(2)}$	0.40(2)	0.49(2)

Note. Bracketed values are precision estimates based on counting statistics.

CONCLUDING REMARKS

Prior to this work, the structure of zirconolite-4M has been thought to be that of zirconolite-2M. Poor fits to neutron powder diffraction data discounted the 2M model. A four-layer model that explained both X-ray and neutron powder diffraction data was determined. This model, zirconolite-4M, describes a four-layer repeat sequence of HTB-type layers. In between these layers are interlayer cations that alternate between those found in zirconolite-2M and those found in pyrochlore. The resulting module sequence alternates between zirconolite-2M and pyrochlore-type modules.

High resolution transmission electron microscopy showed that the four-layer repeat sequence is predominant in the zirconolite-4M specimens. Some regions did deviate from the four-layer repeat sequence; this showed up as smudging in selected area electron diffraction patterns. These stacking anomalies suggests that the energy required to change the stacking sequence of zirconolite-4M is small.

REFERENCES

1. A. E. Ringwood, S. E. Keeson, K. D. Reeve, D. M. Levins, and E. J. Ramm, *in* "Radioactive Waste Forms for the Future" (W. Lutze and R. C. Ewing, Eds.), pp. 233–334. NorthHolland, Amsterdam, 1988.
2. P. E. Fielding and T. J. White, *J. Mater. Res.* **2,** 387–414 (1987).

3. V. M. Oversby and A. E. Ringwood, Rad. Waste Management **1,** 289 (1981).
4. R. Roy, *J. Am. Ceram. Soc.* **60,** 350 (1977).
5. B. C. Chakoumakos, T. Murakami, G. R. Lumpkin, and R. C. Ewing, *Science* **236,** 1556–1559 (1987).
6. K. L. Smith and G. R. Lumpkin, *Geosci. Appl.* 401–422 (1993).
7. A. A. Coelho, "An X-ray and Neutron Diffraction Investigation of Rare Earth Substituted Zirconolite Compounds." Ph.D. Thesis, University of Technology, Sydney, Australia, 1995.
8. T. J. White, *Am. Mineral.* **69,** 1156–1172 (1984).
9. B. M. Gatehouse, I. E. Grey, R. J. Hill, and H. J. Russell, *Acta Crystallogr. Sect. B* **37,** 306–312 (1981).
10. H. J. Rossell, *in* Crystal XII, Abstracts of the 12th Meeting of Crystallographers in Australia, 30 January–2 February 1980," p. 242.
11. H. J. Rossell, *Nature* (*London*) 282–283 (1980).
12. W. Sinclair and R. A. Eggleton, *Am. Mineral.* **67,** 615–620 (1982).
13. P. Bayliss, F. Mazzi, R. Munno, and T. J. White, *Mineral Mag.* **53,** 565–569 (1989).
14. F. Mazzi and R. Munno, *Am. Mineral.* **68,** 262–276 (1983).
15. M. A. Subramanian, G. Aravamudan, and G. V. Subba Rao, *Prog. Solid State Chem.* **15,** 55–143 (1983).
16. J. K. Stalick, *in* "Accuracy in Powder Diffraction II, at NIST, Gaithersburg." Publication **846,** 1992.
17. A Yamamoto, *Acta Crystallogr. Sect. C* **47,** 1588–1591 (1991).
18. R. W. Cheary and A. A. Coelho, *J. Appl. Cryst.* **27,** 673–681 (1994).
19. C. J. Howard, C. J. Ball, L. D. Davis, and M. M. Elcombe, *Aust. J. Phys.* **35,** 507–518 (1983).
20. H. M. Rietveld, *J. Appl. Cryst.* **2,** 65–71 (1969).
21. D. B. Wiles and R. A. Young, *J. Appl. Cryst.* **14,** 149–150 (1981).